ELSEVIER

Journal of Nuclear Materials 281 (2000) 182–190

journal of nuclear materials

www.elsevier.nl/locate/jnucmat

Passivation of uranium towards air corrosion by N_2^+ and C^+ ion implantation

R. Arkush [a], M.H. Mintz [a,b], N. Shamir [a,*]

[a] *Nuclear Research Center – Negev, P.O. Box 9001, Beer-Sheva, Israel*

[b] *Department of Nuclear Engineering, Ben-Gurion University of the Negev, P.O. Box 653, Beer-Sheva, Israel*

Received 4 April 2000; accepted 19 June 2000

Abstract

The passivation of uranium surfaces against air corrosion, by ion implantation processes was studied, using surface analysis methods. Implanting 45 keV N_2^+ and C^+ ions produces thin modified surface layers with gradual gradients of the corresponding compounds (i.e., nitrides and carbides, respectively), which avoid the formation of discontinuous interfaces typical to coatings. Such gradual interfaces impart excellent mechanical stability and adhesion to the modified layers, in spite of the large misfit between the metal substrate and the implantation on induced compounds. It turns out that these layers provide an almost absolute protection against air corrosion. A rapid initial stage of oxidation of the modified surface layers takes place, forming very thin protective oxidation zones (1–4 nm thick), which practically stop further air oxidation for years. The mechanism of the initial oxidation stage of the modified layers seems to vary with the type of surface (i.e., either nitrides or carbides). However, in any case the protection ability of the formed oxidation products is excellent, probably due to the close match between these compounds and the underlying nitrides or carbides.

1. Introduction

Corrosion of uranium by dry and humid air has been extensively studied and reviewed [1,2]. The kinetics and mechanisms of the reaction [3–8] are outside the scope of the present study. In general, the oxidation kinetics of uranium in dry air initially follow a parabolic or linear curve, followed by a linear stage. Swelling of the surface (nodules) was observed in the transition between the two stages by hot-stage-microscopy experiments [9,10]. It was suggested that in the second stage, the oxide cracks and does not behave any longer as a diffusion barrier. For humid air the kinetics are linear for all humidities and the model suggested [8,11] is that of a thin adhesive oxide layer that exists at the oxide–metal interface coated by a porous overlayer that is not protective.

The protection of uranium against air-corrosion is of great importance in nuclear technology, especially for long term storage of non-irradiated components, e.g., in the nuclear fuel manufacture.

Ion implantation is a well-known method for protection of metals against wear, fatigue and corrosion [12]. The subject of ion implantation and thermal oxidation is well treated in the excellent reviews by Dearnaley [13,14]. A couple of studies deal with ion implantation of uranium and U–0.2 w% V for prevention of the hydriding reaction: O_2^- [15], C^+ [16], N_2^-, Si^+ and S^+ [17,18], implanted in various doses and energies, all reduce and slow the hydriding of the metal substrate.

2. Experimental

2.1. Samples

The samples (~10 mm diameter and ~1 mm thick) were of two kinds:

* Corresponding author.
E-mail address: nshamir@hotmail.com (N. Shamir).

0022-3115/00/$ - see front matter
PII: S0022-3115(00)00335-4

(a) nuclear grade pure uranium (less than 300 ppm impurities);
(b) U–0.1%wt Cr. This alloy, developed for nuclear fuel [19,20], has finer and more equi-directional grains than pure uranium [21].

It was found, however, during the present study, that no difference in the corrosion behavior of these two types of uranium was apparent, either for the implanted or for the non-Implanted (non-I) specimens. Hence, no further distinction is made between these samples and both are denoted henceforth as 'uranium'.

2.2. Ion implantation and initial surface oxidation state

Prior to implantation the samples were polished (up to 4000 mesh) and cleaned with an organic solvent. Transfer and storage was made under primary vacuum in the presence of a moisture getter (BaO) that prevented any significant oxidation. The implantation was performed on the MEIRA ion-implanter [22] located at the Soreq Nuclear Research Center. The samples were attached to a water-cooled copper plate and placed in the ion beam line. The maximal temperature measured on the plate during implantation was 80°C. The attachment of the samples by a bolt and a washer produced on the implanted face a masked non-I region, which served as a reference in some of the corrosion measurements.

In the MEIRA implanter, the ions formed by gas ionization in the ion source were mass separated by a magnet and rastered on the sample-plate in order to achieve a homogeneous distribution on all the samples. Two types of ions, N_2^+ and C^+ were implanted. The implantation parameters that were controlled were the energy of implantation (45 keV) and the total implantation dose (6×10^{21} ions/m^2). Simulation calculations (by the TRIM program [23]) indicated these parameters to be the optimal ones to reach a near-stoichiometric nitride or carbide composition, under steady-state conditions established by the concurrent implantation and sputtering processes occurring under irradiation. The thin oxide layer that initially coats the samples (prior to implantation) is sputtered and removed during the ion irradiation, and the (implanted) metal surface moves inwards so that the maximum implant density is obtained on the surface.

The products of the implantation, determined by X-ray diffraction (not presented), were U_2N_3 for the N_2^+ implantation and mostly UC_2 with a small fraction of U_2C_3 for the C^+ one, in accord with literature [16–18].

Following implantation, the samples were stored in encapsulated Pyrex tubes under a vacuum of $\sim10^{-4}$ Torr until the humid-air corrosion experiments were performed. The overall time of exposure to air during handling prior to measurement or reaction (transfer, encapsulation, etc.) was less than 30 min.

Fig. 1 presents the above mentioned TRIM calculated implantation profiles for C^+ and N_2^+ together with the measured Auger electron spectroscopy (AES) profiles (see Section 2.4) performed on two samples (exposed to air for a period of <30 min).

In this figure, the sputtering rate during the depth profile measurements was assumed to be constant and was estimated by coincidence of the points of half-maximum intensities in the measured and in the TRIM calculated profiles. This procedure resulted in an average sputtering rate of 2 nm/min under the applied sputtering conditions. As evident from Fig. 1, the fit between the measured and calculated profiles obtained under this procedure is not good due to the simplified assumption of a constant sputtering rate value. A better calibration approach is discussed further in Section 3.

It can be observed in the figure that, while in the C^+-implanted (CI) sample the carbon profile was almost unaffected by the short air exposure associated with the

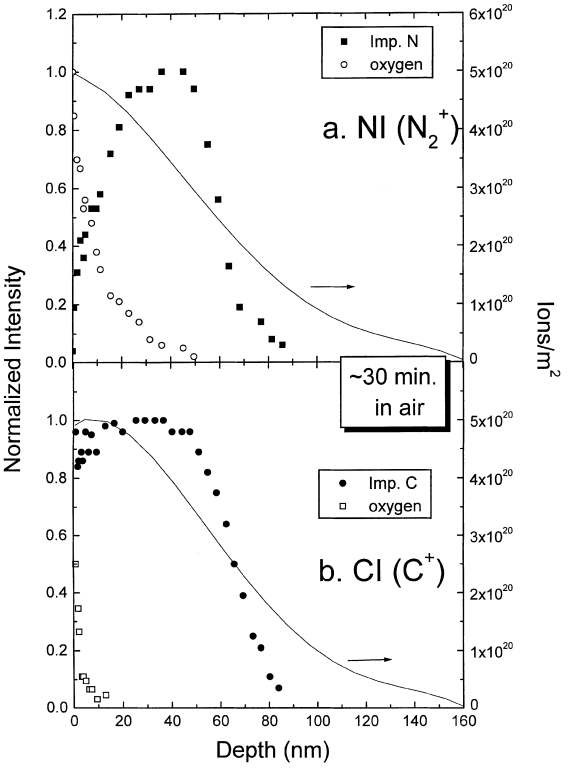

Fig. 1. Normalized experimental (full and empty symbols) and TRIM theoretical (full line) AES depth profiles of implanted uranium samples exposed to air during sample handling: (a) Nitrogen implanted (NI); (b) Carbon implanted (CI). The conversion of experimental sputtering time to a depth scale was done assuming a constant rate, calibrated by coinciding the points of half-maximum intensities in the measured and in the TRIM calculated profiles. The TRIM calculated dose of ion implanted area–concentration is indicated on the right axis.

sample handling and transfer, the nitrogen profile in the N_2^+-implanted (NI) sample was more significantly affected. The oxygen profile in Fig. 1(a) is roughly a 'mirror picture' of the missing nitrogen (compared to the TRIM implantation profile). Hence, atmospheric oxygen is gradually replacing implanted nitrogen. For the CI sample (Fig. 1(b)) it seems that no such substitution occurs. The oxygen surface concentration is about half of that of the saturated NI samples.

The normalization and calibration of the different oxygen intensities was performed as follows:

1. For the NI and non-I samples, the O maximum intensity was normalized to 1. As mentioned before, oxygen replaces nitrogen on the implanted sample, and this substitution is almost complete on the surface. Hence, similar oxygen surface concentrations are anticipated for both NI and non-I surfaces.
2. For the CI samples, the surface oxygen intensity was calibrated by the ratio of surface O/U (CI) to O/U (NI). It turns out that this ratio is about 0.5 (i.e., the oxygen concentration on this surface is about 50% of that on oxidized uranium or oxidized NI samples).

2.3. Oxidation reaction conditions

Two kinds of oxidation reaction conditions were applied:

- Ambient air oxidation over very long periods (up to 5 yr). An average relative humidity of about 40–60% characterizes these ambient conditions.
- Experiments performed in air in sealed Pyrex containers. A constant relative humidity supplier, consisting of a carboxy-methyl-cellulose gel [24], was placed in the containers with different controlled RH values of 80%, 45% and <1%, obtained by the addition of a BaO getter. The humidity values were measured by a gauge, attached to the container for a couple of hours, prior to introduction of the samples. The containers were opened and samples were taken for measurements after three and six weeks. It is estimated that the reduction of oxygen concentration in the sealed volume was not significant during these periods.

Both sets of experiments were performed at ambient temperature. It has to be noted that the two above sets of conditions, both performed under air, practically differed only in the time periods of the reaction and the respective humidity values.

No hydrogen is produced in the gas phase due to the water–metal reaction as long as oxygen is present.

2.4. Experimental techniques

The main experimental technique applied in the present study was AES depth profiling. This technique enables quantitative analysis of all the elements involved as well as their depth distribution. The sputtering was performed using 5 keV Ar^+ ions with a current density of $\sim$30 $\mu A/cm^2$.

In addition, optical photography, scanning electron microscopy (SEM), atomic force microscopy (AFM), X-ray diffraction (XRD) and Fourier transform infrared spectroscopy (FTIR) were applied. The results of the FTIR measurements (not presented) fully corroborated those measured by XRD indicating the formation of uranium dioxide on the non-I surfaces (for the implanted samples, the thickness of the formed oxides, a few nm, is too thin for detection).

3. Results and analysis

As mentioned in Section 2.2, the assumption of a single, constant, sputtering rate, produced a bad fit between the measured and calculated implantation profiles (Fig. 1). In order to correct this fit, two sputtering rates should in fact be used, one for the carbide, nitride and oxide, and another rate for the pure metal. A linear combination of these rates weighted by the relative concentrations of the metallic and non-metallic constituents was then assumed for the mixed region (i.e., the 'tail' of the profile). The result is presented in Fig. 2 and evidently the fit is good. The sputtering rates obtained are 1 nm/min for the non-metallic components and 4 nm/min for metallic uranium. The former sputtering rate closely corresponds to a calibration made by sputtering an oxide layer with a known thickness, (determined independently by optical means [25]), which yielded the same rate under the same sputtering conditions.

Fig. 3 presents a photograph of the interface between the NI and the (washer masked) non-I areas on a sample stored for 5 yr under the ambient atmosphere. The difference between the heavily oxidized non-I area and the shiny implanted area is clearly apparent, indicating the effectiveness of the ion implantation in preventing humid air corrosion. This interface is presented also in a SEM micrograph, Fig. 4, and an AFM micrograph, Fig. 5. Both micrographs emphasize the corroded nature of the non-I surface, in contrast to that of the NI one. The height difference between the two areas (resulting from excessive oxidation of the non-I area) is estimated from the AFM measurements to be around 1.5 μm. Similarly, for the C^+ implanted sample, the qualitative difference in the extent of oxidation (as well as the identification of the constituents formed on the surface by implantation and oxidation) resulted by ambient storage for 3 yr, can be seen in the XRD spectra of the CI and non-I sides, depicted in Fig. 6.

Fig. 7 presents AES depth profiles (calculated by the same procedure mentioned above, using the two sputtering rates) of the NI and CI samples that were kept

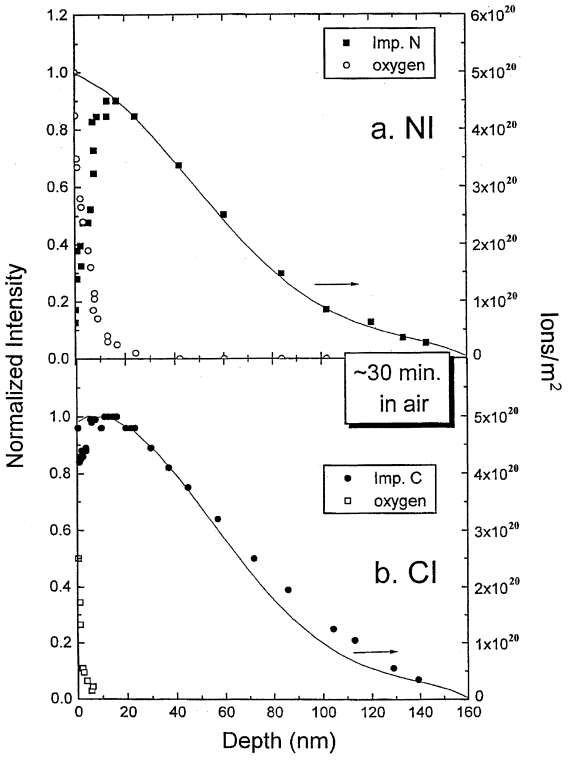

Fig. 2. The correction of experimental sputtering depths utilized in Fig. 1, by assuming two different sputtering rates, one for the non-metallic and another for the metallic constituents. An improved fit is obtained between experimental and TRIM calculated results (symbols as in Fig. 1).

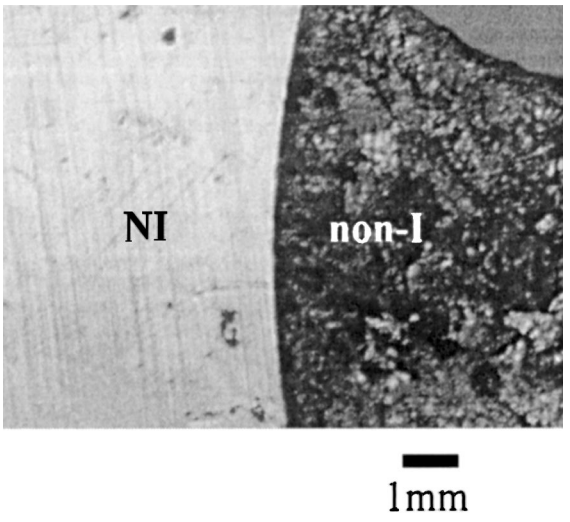

Fig. 3. An optical photograph of the NI and of the non-I interface of a uranium sample that was kept for 5 yr under ambient atmosphere.

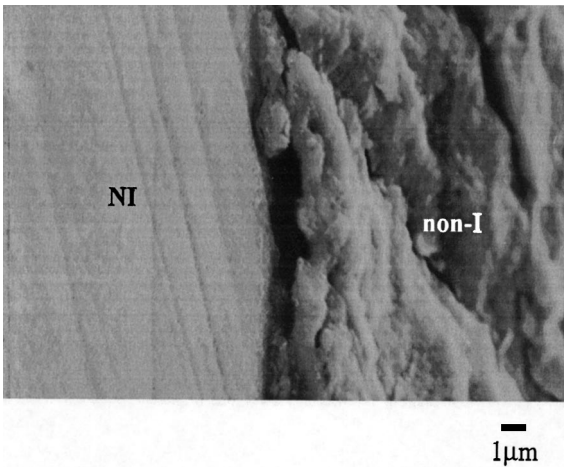

Fig. 4. A SEM micrograph of the NI and the non-I interface of a uranium sample displayed in Fig. 3. A 60° tilting was applied in order to enhance the different roughness of the two areas.

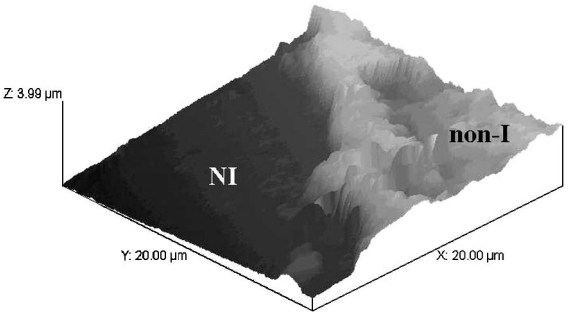

Fig. 5. An AFM micrograph of the NI and of the non-I interface of the uranium sample displayed in Figs. 3 and 4.

under air for three years. Fig. 8 compares the development occurring in the O depth profiles of the implanted samples between 30 min and 3 yr storage under air. Comparing these oxygen profiles, it can be seen that *the oxygen penetration into the NI sample was completed during the first few minutes, and stayed the same* (∼3 *nm*) *for years. For the CI sample, the oxygen penetration during* 3 *years advanced to* ∼3 *nm compared to* ∼1 *nm in* 30 *min*.

Comparing Figs. 2 and 7 it can also be observed that the implantation profile is not absolutely static and some inward diffusion of the implanted N and C occurred during the years.

The non-I face of the samples served as a reference for corrosion of the non-passivated uranium. The oxygen profiles of CI and non-I faces reacted for 14 weeks with <1%, 45% and 80% RH air atmospheres are compared in Fig. 9.

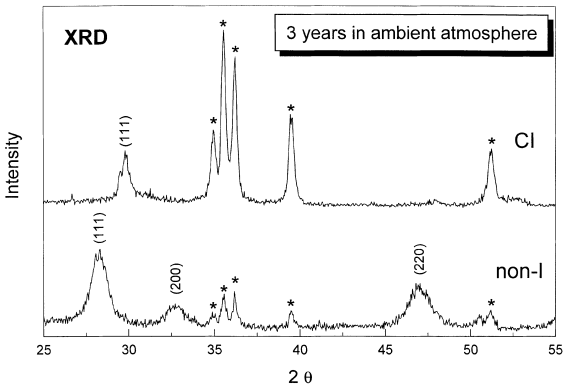

Fig. 6. X-Ray diffraction (XRD) spectra of the CI and of the non-I faces of a uranium sample that was kept for 3 yr under ambient atmosphere. * indicates uranium substrate lines, (1 1 1) in the CI spectrum indicates a UC_2 line and the indices in the non-I spectrum indicate UO_2 lines.

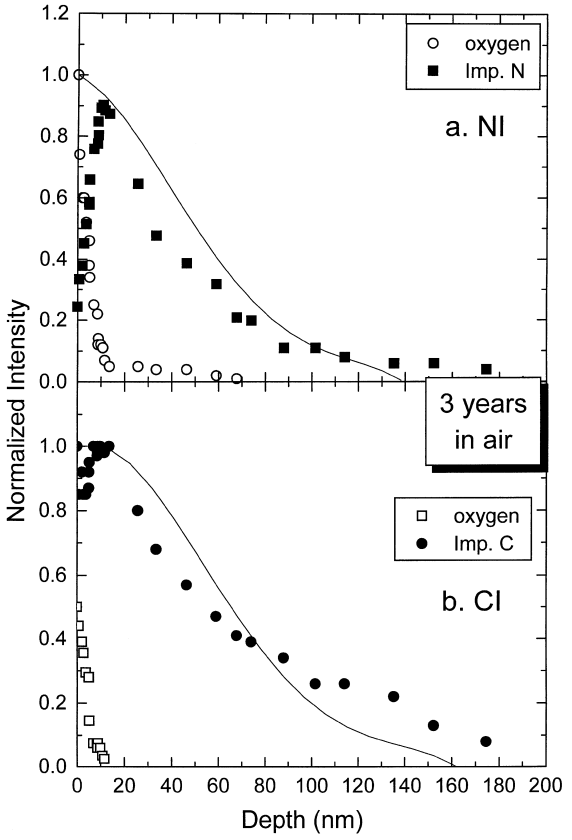

Fig. 7. The normalized experimental AES depth profiles for: (a) NI and (b) CI for samples that were kept for 3 yr under ambient atmosphere. Sputtering depths were determined as in Fig. 2. For comparison the 'zero time' TRIM calculations (Fig. 2) are displayed by the solid lines.

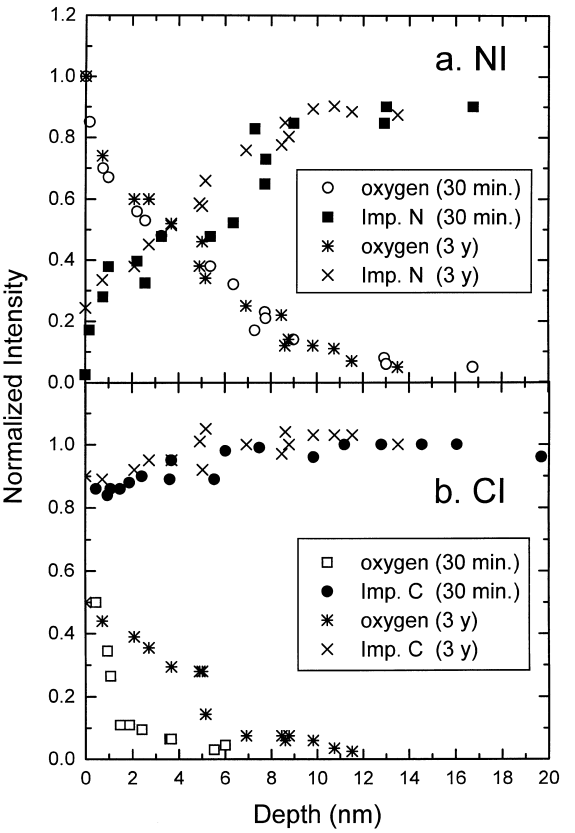

Fig. 8. Unified presentation of the outermost 20 nm depth of Fig. 2 (up to 30 min) and Fig. 7 (3 yr) exposure to ambient atmosphere.

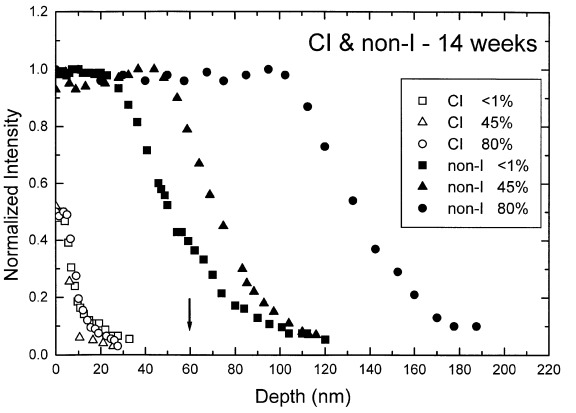

Fig. 9. A comparison between oxygen AES depth profiles obtained for the CI and for the non-I surfaces exposed for 14 weeks to air with different relative humidities (<1%, 45% and 80%). The arrow indicates the C^+ implantation depth (half-maximum concentration).

A number of additional facts can be observed in Figs. 2, 7–9:

- For the non-I samples the oxide development rate is fast and constant (~10 nm/week) for the 80% RH (measurements for 3 weeks not presented). This rate decreases with decreasing relative humidity. N_2^+ and C^+ implantation drastically reduce this penetration rate and also cancel its dependence on humidity (which is about linear between 45% and 80% RH for non-I uranium).
- For the CI samples, the initial oxidation rate is less than half of that for the NI samples (Fig. 2). Since the oxygen concentration on the CI surface is half of that on the NI surface, the integral amount of penetrating oxide is, hence, about a quarter of that for the NI samples. In 3 years the depth is about equal (~4 nm, Fig. 8) for both NI and CI, so in the very long run, nitrogen implantation probably provides a better passivation than carbon implantation.

As described above, a rapid formation of a thin oxide layer (1–4 nm thick), which provides a very effective protection for further air oxidation, occurs on the ion-implanted samples. It has been observed that the duration of the initial process is less than the handling time of the implanted samples (ca. 30 min). In order to establish more accurately this time scale, in situ oxidation of sputtered (oxide-free) implanted samples was performed in the UHV Auger system. In these experiments the native oxide layer present on the samples was removed by Ar^+ ion sputtering. This surface was then exposed to 5×10^{-8} Torr O_2 for the NI sample and 5×10^{-9} Torr O_2 for the CI one, monitoring continuously the AES peak intensity of the implanted species (i.e., either N or C), oxygen and uranium. For comparison, similar experiments were conducted on a sputter-cleaned, non-I uranium surface.

Fig. 10 summarizes the O_2 exposure behavior of the NI, as compared to the non-I surfaces. It can be seen that oxygen rapidly replaces the N atoms on the

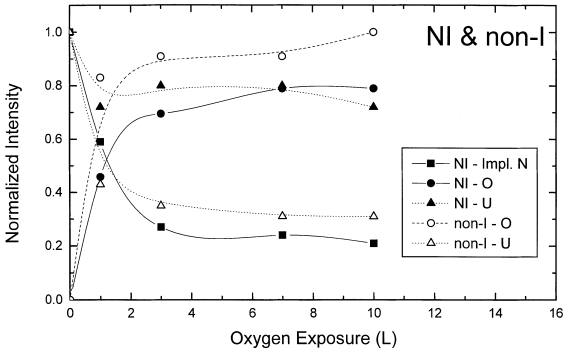

Fig. 10. Normalized O, N and U AES intensities vs low-pressure oxygen exposure of the NI and the non-I surfaces.

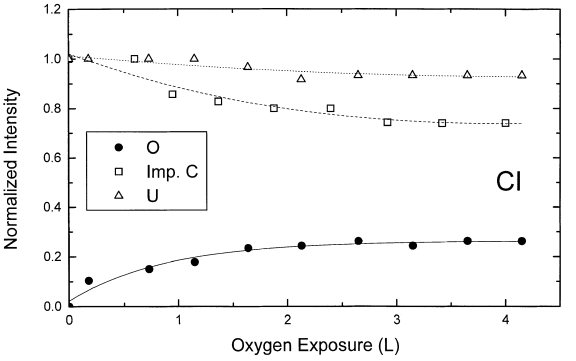

Fig. 11. Normalized O, C and U AES intensities vs low-pressure oxygen exposure of the CI surface.

implanted surface, forming a thin oxide layer (1–2 nm, i.e., 3–6 monolayers) within an exposure of about 4–5 Langmuirs (1 L = 10^{-6} Torr s). This thickness is estimated from the AES nitrogen peak at saturation, assuming that the electron mean free path is about 7 Å [26]. The kinetics of this oxidation process is in fact quite similar to that of the non-I surface, as indicated by the similar exposure behavior of the this surface. It should be realized that the 'saturation' behavior displayed in these exposure curves for all samples (occurring above 4 L exposure) is in fact not a real saturation since the oxidation reaction still proceeds to some extent, though at a significantly lower rate. True saturation is obtained for the implanted samples (especially the NI) only after oxidation of about 4 nm (i.e., ~13 monolayers) is obtained. Evidently, no such real saturation is reached for the non-I surface, where oxidation proceeds for long term periods.

The corresponding initial oxidation kinetics of the CI sample are presented in Fig. 11. This kinetics is similar to the above kinetics of nitride to oxide conversion (saturation at about 4 L). However, in contrast to the oxide layer formed on the NI sample after the 4–5 L exposure that was estimated to be 4–6 monolayers thick, the species formed on the CI sample at that exposure is estimated to consist of only one oxygen monolayer, i.e., the possible formation of UCO.

The reaction probability in these cases correspond to ~100% efficiency (every impinging oxygen molecule reacts) for nitride to oxide conversion and to ~20% for carbide oxidation. It should be noted again that these coefficients are related only to the very initial stage of oxidation till the formed passivation layer is completed.

4. Discussion

It has been demonstrated (Figs. 7–9) that the oxide growing on the surface of non-I uranium is non-

protective, resulting in about a linear growth with a significant dependence of the growth rate on the level of humidity (Fig. 9). The passivation of uranium towards humid air corrosion by ion implantation is clearly demonstrated by the AES depth profiles (Figs. 6–9) performed on the NI and CI samples reacted with air at various humidities. For both NI and CI samples, the implantation practically stops the oxidation process after a few minutes of exposure, for all humidity levels.

In spite of the similar passivation effectiveness of the two types of implantation species (i.e., N and C) there are still some substantial differences between the initial oxidation behavior of the two modified surfaces. The initial oxide advance into the N_2^+ implanted layers seems to be at the expense of the surface nitride, i.e., oxygen from the reacting air replaces nitrogen with ~100% efficiency:

$$2U_2N_3 + 4O_2 \rightarrow 4UO_2 + 3N_2 \quad (1a)$$

or

$$2U_2N_3 + 7O_2 \rightarrow 4UO_2 + 6NO \quad (1b)$$

This is evident from Figs. 8 and 10, in which the O and N lines are 'mirror images' of each other.

The type of kinetic curves displayed in Figs. 10 and 11 seems to indicate that the rate of this gas-surface reaction process is controlled by the dissociative chemisorption step on the unreacted (sputter-cleaned $UN_2 + U_2N_3$) area [27]. If we denote the reacted fraction of the surface (i.e., that is already coated by reaction product islands) by α, the chemisorption rate is then given by

$$\frac{d\alpha}{dt} = k(1-\alpha), \quad (2)$$

where k is the reaction constant, which leads to the exponentially decaying kinetics, observed in Figs. 10 and 11. If on the other hand the rate-controlling step of the reaction had been at the product island boundaries, sigmoidal type kinetics would be displayed, as common in many solid state nucleation and growth phase transformations [28].

The high efficiency of the reaction through the ~5 L exposure range probably points to the formation of ~5 monolayer islands, growing laterally, so that the oxygen reaction proceeds directly at the island edges (not involving diffusion through the product oxide). This process reaches quasi-saturation when the islands coalesce to form a full layer. Afterwards the oxidation slowly continues inwards by the diffusion of (dissociated) oxygen through the thin oxide. The process completely stops at a thickness of about 13 monolayers. For the C^+ implanted layer, the process is more complicated. In the first step (Fig. 11 – exposure to a couple of Langmuirs of oxygen) oxygen replaces one of the two carbons in the first monolayer and the process reaches quasi-saturation. In a later step (exposure to air for time periods between minutes and years) oxygen penetrates through the oxidation product layer and reacts slowly with the carbide. The C(AES) intensity, however, does not vanish concurrently with this oxygen accumulation process (Figs. 8 and 11). Hence the process is probably that the oxygen, penetrating through the initially reacted layer either reacts with the carbide forming an oxy-carbide [29,30], or replaces the carbon (similarly to the initial step) leaving unbound carbon atoms (or clusters) in the solid. The latter possibility seems less likely since formation of atomic C in the presence of oxygen should lead to a recombination reaction and the release of CO, which is thermodynamically favorable.

The formation of an oxy-carbide compound also accounts for the different behavior of the NI and the CI samples. Such a compound exists only for the U–C–O ternary system [29,30] and has not been identified for the U–N–O one. Hence, for the NI case, only the pure uranium oxide can be formed in the solid (i.e., the total replacement of nitrogen in the nitride by oxygen) whereas, for the CI case, oxygen may form the oxy-carbide compound, leading to the accumulation of oxygen without the concomitant disappearance of all the carbon. The saturation concentrations of oxygen in these two cases (which as described in Section 2 is lower by a factor of about 2 for the CI samples) is also consistent with the formation of UO_2 for the NI samples and UOC for the CI ones. It can thus be concluded that for the carbon-implanted samples, the reaction controlling the oxidation process is

$$UC_2 + O_2 \rightarrow UOC + CO \quad (3)$$

In contrast to the symmetry observed in the oxygen/nitrogen depth profiles of the oxidized NI samples, stemming from the substitution of N by O, there is no symmetry in the oxygen–carbon intensity profiles for the CI sample (Figs. 1, 2, 7, 8). This results from the presence of adventitious carbon present on the surface of the oxidized surfaces.

The initial oxy-carbide formation rate is significantly lower than that of the oxide formation on the NI surface (Fig. 11) and an oxy-carbide layer of about 10 nm is formed after 3 yr under ambient atmosphere (~40% RH average) or 14 weeks of reaction with 80% humid air. This thickness is about half of that of the oxide formed on the NI sample in a coupled of minutes. The NI therefore initially provides less protection than the CI, as can be observed in Figs. 1, 2, 7, 8, but the oxide formed on the NI surface seems to provide perfect protection since *absolutely* no more penetration occurs after the completion of a (~13 monolayers thick) continuous oxide layer. On the other hand, the

oxy-carbide formed on the CI surface slowly advances with time and in three years reaches the depth of the NI oxide (Fig. 8). In the long run (more than 5 yr) it seems that nitrogen implantation provides the best protection, though practically carbon implantation also provides a comparable passivation. In contrast, the oxidation of the non-I sample reaches about 150 nm during 14 weeks of exposure to 80% RH air (Fig. 9) and >1 μm after 3 yr under ambient atmosphere (not presented in the figures).

The extreme corrosion resistance imparted by the ion modification processes, as compared with the non-I case, may be accounted for by the similar structure and density of the surface compounds, formed by these implantation processes, to that of UO_2. The very good lattice match of the oxidation-formed oxide (or oxy-carbide) and that of the ions-formed substrates (UC_2–UN_2– results in an almost coherent and adhesive oxidation layer without the cracks flaws and faults typical to the oxide on the non-I where a significant mismatch of ~40% exists.

It may be argued that a significant mismatch still exists between the nitride or carbide, produced by the ion-implantation, and the metal beneath, so that a strained, defected structure of the modified surface zone (even before oxidation) is anticipated. However, in contrast to the case of an oxidation front that is terminated by a sharp discontinuous oxide–metal interface, the ion implantation process produces a wide interface zone where a gradual change of the metallic to non-metallic constituents exists (e.g., Fig. 2). This diffuse interface stabilizes the transition between the pure metal and the pure non-metallic surface compounds, without inducing the strained defected structure in the latter. Hence, the following air oxidation takes place on an adhesive, non strained substrate (i.e., nitride or carbide), which, as mentioned before, matches the structure of the oxidation product.

5. Summary and conclusions

N_2^+ and C^+ implanted (NI and CI, respectively) samples as well as non-I reference samples were exposed to air with controlled <1%, 45% and 80% relative humidities for 14 weeks and to atmospheric air for 3–5 yr. Also, controlled in situ low-pressure exposures to oxygen were conducted in a surface-analysis system. The reacted samples were analyzed by the AES, XRD and FTIR techniques and the main results are:

1. Nitride and carbide layers are formed by N_2^+ and C^+ implantations, respectively, having gradual concentration gradients in the implanted-layer/metal interface. These gradients avoid the formation of sharp discontinuous interfaces, hence produce modified surface zones with good mechanical stability.
2. During a short (~5 L) in situ exposure to oxygen an oxide layer, ~5 mono-layers thick is formed on the nitride and a one monolayer oxy-carbide is formed on the carbide.
3. The initial oxidation reaction mechanism is different for both implanted surfaces. For the NI surface, oxygen replaces all nitrogen atoms of the nitride (forming oxide islands, about 5 monolayers thick, spreading on the surface). For the CI surface only half of the carbon atoms is replaced by oxygen (forming a layer by layer development of an oxy-carbide).
4. During a few minutes of exposure to ambient air, the oxide layer on top of the NI surface thickens to ~13 monolayers providing *absolute passivation* (i.e., no more advance of the oxide occurs for 5 yr). For the CI surface, ~5 mono-layers of oxy-carbide are formed after a few minutes, continuing to grow slowly. In 5 yr its thickness is comparable to that of the NI oxide, providing practically about the same protection.
5. It is proposed that the excellent passivation provided by the implantation layer stems from its gradual transition from the metal substrate to the stoichiometric nitride or carbide. This gradual transition forms a diffuse interface that helps to join the two mismatching structures (i.e., the metallic and non-metallic). The oxide (or oxy-carbide) formed on the implanted non-metallic layer is a good crystallographic match with the substrate. Hence, this oxide provides an excellent barrier against further oxidation.

In conclusion, ion implantation was demonstrated to be an effective technique for protection of uranium towards corrosion.

From the practical view, the ion-implantation method is economically and technically restricted to small items, having simple shapes, which need special protection. Plasma nitridization and carbonization can be applied to achieve a similar protection on a wider scale. Such treatment was reported [31] to provide good protection (even better than the 45 keV ion-implantation) against hydrogen attack and preliminary results indicate also good protection against humid air corrosion, so the technique seems to be promising. Plasma treatment implants the sample (in a totally different process) with ions of much lower energy (in the eV range). Consequently, before trying this application, it has to be studied in detail whether the effective passivation due to the special conditions of the 45 keV implantation, applied in the present study (causing a specific profile of radiation defects and hence possibly nucleation sites), can also be achieved with comparable effectiveness by plasma treatments.

Acknowledgements

We would like to acknowledge Dr G.D. Lempert for the performance of ion implantations, Mr S. Zalkind for the SEM micrographs and Mr Z. Katchalski for the AFM micrographs. This work was partially supported by a grant from the Israel Council for Higher Education and the Israel Atomic Energy Commission.

References

[1] A.G. Ritchie, J. Nucl. Mater. 102 (1981) 170.
[2] C.A. Colmenares, Prog. Solid State Chem. 15 (1984) 257.
[3] A.G. Ritchie, R.C. Greenwood, S.J. Randles, J. Nucl. Mater. 139 (1986) 121.
[4] J.E. Antill, M.J. Bennett, K.A. Peakall, B.L. Myatt, J. Nucl. Mater. 50 (1974) 2.
[5] M.J. Bennett, B.L. Myatt, D.R.V. Silvester, J.E. Antill, J. Nucl. Mater. 57 (1975) 221.
[6] S. Orman, G. Picton, J.C. Ruckman, J. Oxide Met. 1 (1969) 199.
[7] G.W. McGillivray, D.A. Geeson, R.C. Greenwood, J. Nucl. Mater. 208 (1994) 81.
[8] A. Danon, J. Koresh, M.H. Mintz, Langmuir 15 (1999) 5913.
[9] L. Leibowitz, J.G. Schnizlein, L.W. Mishler, R.C. Vogel, J. Elec. Soc. 108 (1961) 1153.
[10] L. Leibowitz, J.G. Schnizlein, J.D. Bingle, R.C. Vogel, J. Elec. Soc. 108 (1961) 1155.
[11] E.W. Haycock, J. Electron Soc. 106 (1959) 771.
[12] I.J.R. Baumvol, in: J.F. Ziegler (Ed.), Ion Implantation Science and Technology, Academic Press, Orlando, FL, 1984, p. 261.
[13] G. Dearnaley, in: J.R. Hirvonen (Ed.), Treatise on Materials Science and Technology, Vol. 18: Ion Implantation (chapter 7).
[14] G. Dearnaley, J. Nucl. Mater. 182&183 (1981) 899.
[15] R.G. Musket, G. Robinson-Weis, R.G. Patterson, UCRL-89360, 1983.
[16] R.G. Musket, UCRL-95609, 1987.
[17] A. Ayral, D. Crusset, G. Raboisson, Mater. Res. Soc. Symp. Proc. 268 (1992) 9.
[18] D. Crusset, PhD thesis, Université de Bourgogne, Dijon, 1992 (in French).
[19] H. Aubert, Mem. Scien. Rev. Metallurg. 58 (1961) 276.
[20] M. Englander, Rapport CEA No 776, CEN de Saclay, 1958.
[21] W.D. Wilkinson, Uranium Metallurgy, Vol. II: Uranium Corrosion and Alloys, Wiley Interscience, New York, 1962, p. 875.
[22] G.D. Lempert, Surf. Coat. Technol. 34 (1988) 185.
[23] J.P. Biersack, L.G. Haggmark, Nucl. Instrum. and Meth. 174 (1980) 257.
[24] A. Bettelheim, J. Hayon, S. Weiss, Z. Chernia, R. Ydgar, D. Ozer, J. Electroanal. Chem. 405 (1996) 251.
[25] Z. Chernia, unpublished results.
[26] P.W. Palmberg, Anal. Chem. 45 (1973) 549A.
[27] D.A. King, M.G. Wells, Proc. Roy. Soc. London A 339 (1975) 245.
[28] J.W. Christian, The Theory of Transformations in Metals and Alloys, Part I – Equilibrium and General Kinetic Theory, 2nd Ed., Pergamon, New York, 1975.
[29] G.C. Allen, P.M. Tucker, J. Chem. Soc., Dalton Trans. 5 (1973) 470.
[30] T. Gouder, C.A. Colmenares, J.R. Naegele, J.C. Spirlet, J. Verbist, Surf. Sci. 264 (1992) 354.
[31] A. Raveh, R. Arkush, S. Zalkind, M. Brill, Surf. Coat. Technol. 82 (1996) 38.